

## SEEKING THE LOCAL CONVERGENCE DEPTH. V. TULLY-FISHER PECULIAR VELOCITIES FOR 52 ABELL CLUSTERS

DANIEL A. DALE,<sup>1</sup> RICCARDO GIOVANELLI, AND MARTHA P. HAYNES

Center for Radiophysics and Space Research and National Astronomy and Ionosphere Center, Cornell University, Ithaca, NY 14853

LUIS E. CAMPUSANO

Observatorio Astronómico Cerro Calán, Departamento de Astronomía, Universidad de Chile, Casilla 36-D, Santiago, Chile

AND

EDUARDO HARDY

National Radio Astronomy Observatory, Casilla 36-D, Santiago, Chile

Received 1999 April 27; accepted 1999 July 9

### ABSTRACT

We have obtained *I*-band Tully-Fisher (T-F) measurements for 522 late-type galaxies in the fields of 52 rich Abell clusters distributed throughout the sky between  $\sim 50$  and  $200 h^{-1}$  Mpc. Here we estimate corrections to the data for various forms of observational bias, most notably Malmquist and cluster population incompleteness bias. The bias-corrected data are applied to the construction of an *I*-band T-F template, resulting in a relation with a dispersion of 0.38 mag and a kinematic zero point accurate to 0.02 mag. This represents the most accurate T-F template relation currently available. Individual cluster T-F relations are referred to the average template relation to compute cluster peculiar motions. The line-of-sight dispersion in the peculiar motions is  $341 \pm 93 \text{ km s}^{-1}$ , in general agreement with that found for the cluster sample of Giovanelli and coworkers.

*Key words:* cosmology: observations — distance scale — galaxies: distances and redshifts

### 1. INTRODUCTION

Deviations from smooth Hubble flow arise as a result of large-scale density fluctuations. Qualitatively, a “convergence depth” is the distance out to which significant contributions to a galaxy’s peculiar motion are made. In linear theory, the fraction of the peculiar velocity of a galaxy, contributed by the mass distribution within a radius  $R$ , can be written as

$$V(R) \simeq \frac{H_0 \Omega_0^{0.6}}{4\pi} \int \delta(r) \frac{\hat{r}}{r^2} W(R) d^3r, \quad (1)$$

where the Hubble constant  $H_0 = 100 h \text{ km s}^{-1} \text{ Mpc}^{-1}$ ,  $\Omega_0$  is the cosmological matter density parameter,  $\delta$  is the mass overdensity, and  $W(R)$  is a window function of width  $R$  (a Gaussian or top-hat, for example) centered at  $r = 0$  (Peebles 1993). If the distribution of matter approximates homogeneity on larger scales, then contributions to the peculiar velocity will eventually taper off with increasing distance.

Observational estimations of the local convergence depth are facilitated through measurements of the reflex motion of the Local Group with respect to spherical shells of increasing radii. The first such program was carried out by Rubin et al. (1976) on an all-sky sample of 96 Sc galaxies between redshifts of 3500 and 6500  $\text{km s}^{-1}$ . They reported the motion of the Local Group with respect to the shell of galaxies was  $454 \pm 125 \text{ km s}^{-1}$  toward  $(l, b) = (163^\circ, -11^\circ)$ , significantly different from the apex of the cosmic micro-

wave background (CMB) dipole, suggesting a large bulk flow for the shell and a convergence depth significantly larger than  $\sim 50 h^{-1}$  Mpc. Subsequent work in this area has yielded conflicting results.

The situation can be grossly expressed into two main views. A picture of a *small* convergence depth ( $cz < 5000 \text{ km s}^{-1}$ ) was first suggested by Tammann & Sandage (1985) and successively by Dressler et al. (1987) and Lynden-Bell et al. (1988). This picture is also supported by early measurements of the distribution of *IRAS* and optical galaxies (Lahav, Lynden-Bell, & Rowan-Robinson 1988; Lynden-Bell, Lahav, & Burstein 1989; Strauss et al. 1992; Hudson 1993). It should be mentioned, however, that some *IRAS* dipoles suggest significant contributions to the Local Group motion arise from the distribution of objects between 5000 and 10,000  $\text{km s}^{-1}$  (e.g., Rowan-Robinson et al. 1990). The latter studies profit from flux dipoles or a peculiar velocity field that is solved for iteratively, initially supposing that recession velocities are indicative of distance and that light traces mass. The above observational programs that utilize this technique find 80% or more of the Local Group motion derives from matter within  $\sim 50 h^{-1}$  Mpc.

Proposals for a *large* convergence depth ( $cz > 10,000 \text{ km s}^{-1}$ ; Scaramella, Vettolani, & Zamorani 1994; Brunozzi et al. 1995; Branchini & Plionis 1996; Plionis & Kolokotronis 1998), mainly resulting from a similar analysis of the distribution of clusters of galaxies, suggest that much of our motion may be produced by mass concentrations as far as  $\sim 13,000 \text{ km s}^{-1}$  (e.g., the “Shapley supercluster”). The latter view is corroborated by reports of bulk motion in the local universe (within 6000  $\text{km s}^{-1}$ ) via Tully-Fisher (T-F) measurements by Willick (1990), Courteau et al. (1993), and Mathewson, Ford, & Buchhorn (1992), and by the recent

<sup>1</sup> Current address: IPAC, California Institute of Technology, 100-22, Pasadena, CA 91125.

analysis of the dipole of cluster brightest elliptical galaxies by Lauer & Postman (1994, hereafter LP). The LP claim, based on the peculiar motions of all Abell clusters to 15,000 km s<sup>-1</sup>, suggests the local volume of space within  $\sim 100 h^{-1}$  Mpc is traveling toward  $(l, b) = (343^\circ, +52^\circ)$  at 689 km s<sup>-1</sup>. The disagreement between these competing views of the convergence depth scale is wide, with important implications for cosmological models, which are generally unable to accommodate bulk flows with scales as implied by the large convergence depth camp (e.g., Gramann et al. 1995).

Fresh work from Hudson et al. (1999) and Willick (1999) challenge the direction of the LP bulk flow vector. Hudson et al. employ the fundamental-plane relation for some 700 elliptical galaxies in 56 clusters ( $3000 \text{ km s}^{-1} \lesssim cz \lesssim 14,000 \text{ km s}^{-1}$ ) to find a bulk flow of  $630 \pm 200 \text{ km s}^{-1}$  in the direction  $(l, b) = (260^\circ, -1^\circ)$ . A bulk motion of  $\sim 700 \pm 250 \text{ km s}^{-1}$  toward  $(l, b) = (272^\circ, 20^\circ)$ , originating from T-F measurements in 172 cluster galaxies ( $9000 \text{ km s}^{-1} \lesssim cz \lesssim 13,000 \text{ km s}^{-1}$ ) and 72 other galaxies ( $cz < 30,000 \text{ km s}^{-1}$ ), is claimed by Willick. Such large bulk flows are not consistent with other recent observational work. Riess, Press, & Kirshner (1995) used observations of 13 Type Ia supernovae and found evidence for a small local bulk flow. In a contribution based on T-F distances of about 2000 galaxies within 9500 km s<sup>-1</sup>, Giovanelli et al. (1998b) similarly report evidence against the existence of a large-scale local flow, and support for a relatively small convergence depth. Many of the aforementioned studies cannot convincingly exclude the existence of large-scale bulk flows, because their sampling is either too sparse (Watkins & Feldman 1995) or of limited depth. This is particularly important in view of the claims that asymptotic convergence of the Local Group reflex motion may only be reached at distances well in excess of 10,000 km s<sup>-1</sup> (Scaramella et al. 1994; Brunozzi et al. 1995; Branchini & Plionis 1996). This work aims at the direct determination of the T-F relation for an all-sky cluster set extending to distances exceeding the highest reported values of the convergence depth.

In addition to ensuring that our T-F relation is valid for usefully large distances, a second issue of concern regards the amplitude of systematic errors in the T-F template. The Giovanelli et al. (1998b) sample of peculiar velocities obtained using the T-F method is referred to a template relation based on the SCI sample, a collection of 782 T-F measurements in the fields of 24 separate clusters between 1000 and 9000 km s<sup>-1</sup> (Giovanelli et al. 1997a, 1997b, hereafter G97a and G97b, respectively). Though the relative proximity of the SCI allows a broad stretch of observable galactic properties and thus makes it an ideal sample to study several characteristics of the T-F template relation, it has limits as to how accurately the relation's zero point can be pinned down. A larger and deeper cluster sample has two main advantages. First, the increased number of clusters reduces the impact of statistical "shot noise." In addition, since the magnitude offset produced in the T-F diagram by a given peculiar velocity decreases with the target distance, the scatter produced by peculiar velocities of distant clusters about the template relation is reduced; thus they are better suited to determining the template relation's zero point. Here we present the results of a program designed to probe the large-scale peculiar velocity field to  $\sim 200 h^{-1}$  Mpc, consisting of spectroscopic and photometric data for an all-sky sample of 522 galaxies from the fields of 52 clus-

ters between  $\sim 50$  and  $200 h^{-1}$  Mpc (hereafter the SCII sample).<sup>2</sup>

The overall scatter of the *I*-band T-F relation of about one-third of a magnitude translates to an uncertainty of 15% in redshift-independent distance measurements. This means that for an individual galaxy at, say, 15,000 km s<sup>-1</sup>, the method is able to predict the distance to within 2250 km s<sup>-1</sup>. This value is considerably larger than the typical value of peculiar velocities, which are of order 500 km s<sup>-1</sup> or less. Even if 50 objects per cluster were to be measured, the distance of a cluster at 15,000 km s<sup>-1</sup> would not be characterized to better than  $2250/50^{1/2} \sim 300 \text{ km s}^{-1}$ ; our measurements include many fewer galaxies per cluster field, typically 10, some of which turned out to be cluster members. The main purpose of this study was thus *not* the determination of accurate *individual* peculiar velocities of remote clusters, but rather to combine measurements in many clusters to obtain a global solution for the dipole of the velocity field.

This is the fifth paper in our series on the local convergence depth. The observational data are presented in Dale et al. (1997, 1998, 1999b, hereafter Papers I, II, and IV, respectively; the data can be obtained by contacting D. A. D.). The core result of this work, that the local dipole flow to about  $200 h^{-1}$  Mpc is consistent with a null bulk motion, is described in Dale et al. (1999a, hereafter Paper III). Details of the sample and its selection are covered in § 2 of this work, while § 3 covers the construction of the universal T-F template relation. Results for the peculiar velocity sample are given in § 4, and we summarize our findings in § 5.

## 2. SAMPLE SELECTION

Clusters of galaxies are used as increasingly pliant tools in cosmology. For our particular concern, the cluster peculiar velocity distribution reliably matches that of the underlying smoothed matter's velocity distribution (Bahcall, Cen, & Gramann 1994a; Bahcall, Gramann, & Cen 1994b; Gramann et al. 1995). Furthermore, though observations of clusters of galaxies only sparsely sample the large-scale velocity field, they can do so more accurately than individual galaxies can. This advantage arises because measurements of many galaxies *within a single bound system* can be made. As peculiar velocities are driven by gravitationally growing density fluctuations, precise comparisons of large-scale peculiar velocities can be made with those predicted by cosmological theories (Watkins & Feldman 1995; Cen, Bahcall, & Gramann 1994; Feldman & Watkins 1994; Strauss et al. 1995; Croft & Efstathiou 1994; Borgani et al. 1997).

### 2.1. Sample Definition

Clusters of galaxies are practical T-F targets. Their outskirts are well populated by spiral galaxies; thus, a small number of wide-field images with a modestly sized telescope can effectively "map" a cluster, and they will likely contain numerous T-F candidates.

<sup>2</sup> The SCI and SCII are complementary samples of cluster T-F data. The SFI is a completely independent sample of T-F data for some 2000 field galaxies. Details on the SCI and SFI samples can be found in Giovanelli et al. (1998a, 1998b) and references therein.

A second consideration that suggests the use of clusters in T-F experiments is the determination of the T-F template. As will be outlined in § 3.1, the template is preferentially measured within a cluster, or determined as an average of templates from measurements in separate clusters. The template slope is best measured if a broad dynamic range of T-F parameters can be observed, preferentially obtained from a relatively nearby sample. In contrast, the kinematic zero point is better characterized at higher redshifts, where cosmic peculiar motions play a smaller role in shifting objects away from the template. Our motive of improving the T-F zero-point accuracy plays an important role in characterizing the redshift distribution of our sample.

A third advantage to using clusters of galaxies in T-F work is the  $\sim\sqrt{N}$  increase in statistical accuracy per cluster they afford if  $N$  T-F measurements per cluster are available—the estimate of a system’s peculiar motion is more accurate when information from multiple objects is used, the distance differential between galaxies in a cluster being negligible for our sample. However, if an all-sky survey of peculiar motions is the goal, concentrating observations to a single cluster or to a small number of clusters parallels an increase in overall sample sparseness. The choice between a densely sampled volume of low-accuracy peculiar velocities and a sparse sample of accurate peculiar velocities ultimately depends on the particular goals of the study.

We early on investigated what sample characteristics would facilitate the most accurate determination of the T-F zero point and the local bulk flow. To ascertain the optimal distribution of clusters and number of galaxies per cluster to observe, we relied on numerical simulations. The only limitation enforced was the total number of objects that could be observed, for target accuracy and a reasonable project timescale. A wide range in the number of clusters and the number of objects per cluster was explored. A variety of models of the peculiar velocity field (multiattractor, linear bulk flows, quiescent, etc.) was imposed, and different models for the shape of the zone of avoidance (ZOA) were considered. These studies profited from numerical simulations of various types of cold dark matter models kindly provided by S. Borgani (see Paper III for further details). T-F errors were assigned using random Gaussian deviates of the scatter distribution in G97a. The results, which took into consideration that clusters of galaxies have positions that are correlated in space (and therefore a random choice of  $N$  clusters does not guarantee that  $N$  independent points are sampled), suggested that about 50 clusters of galaxies needed to be observed, with measurements of at least seven to eight T-F galaxy distances in each.

## 2.2. Cluster Selection

The initial characterization of the SCII cluster sample predates this study and originates from preparatory work done by R. G. for the SCI T-F study. Clusters were selected using the Abell rich cluster catalog as a guide (Abell, Corwin, & Olowin 1980, hereafter ACO). Expediency played an important role in choosing the parent sample of clusters, of which this sample is a subset. Nearby clusters ( $cz \lesssim 10,000$  km s<sup>-1</sup>) with preexisting H I velocity widths and *I*-band fluxes were favored, and the more distant clusters ( $cz \gtrsim 10,000$  km s<sup>-1</sup>) that already had a large number of redshifts available were likewise strongly considered, as that availability improved the prospects for their kinematic

characterization. Table 1 lists the main parameters of the 52 chosen clusters for this work. The parameters listed include the following:

*Column (1).*—Standard name according to the Abell/ACO catalog.

*Columns (2), (3), (4).*—Adopted coordinates of the cluster center, for the equinox B1950.0; they are obtained from ACO, except for the entries A1983b and A2295b, systems found to be slightly offset from A1983 and A2295 in both sky position and redshift.

*Columns (5) and (6).*—Systemic velocities in the heliocentric and in the cosmic microwave background reference frame, respectively, where we assume the motion of the Sun with respect to the CMB is 369.5 km s<sup>-1</sup> toward  $(l, b) = (264.4, 48.4)$  (Kogut et al. 1993). For all the clusters we derive a new systemic velocity, combining the redshift measurements available in NED<sup>3</sup> with our own measurements. An estimated error for the systemic velocity is parenthesized after the heliocentric figure.

*Column (7).*—The number of cluster member redshifts used in determining systemic velocities.

*Column (8).*—Abell richness class.

*Column (9).*—Bautz-Morgan code (Bautz & Morgan 1970) as listed in the ACO catalog.

Figure 1 displays the sample in Galactic coordinates. The symbol sizes are inversely proportional to the cluster redshifts; two examples are given in the lower left for scale. An alternative display of the sample is shown in Figure 2, a stereographic view of the sample in Galactic Cartesian coordinates. The dashed circles have radii of 5, 10, and  $15 \times 10^3$  km s<sup>-1</sup>, and the solid lines in the  $(X, Z)$  and  $(Z, Y)$  plots are for  $|b| = 20^\circ$  and identify the ZOA. This distribution recalls our first criterion in selecting the sample: The data set should uniformly sample as much of the sky as prudently feasible. Since the main thrusts of this work are to recover a bulk flow measurement and to accurately determine a kinematic offset even in the presence of such a flow, an all-sky sample is required. Unfortunately, the paucity of clusters and the large and uncertain Galactic extinction in the direction of the ZOA prohibit us from sampling that portion of the sky. In addition, the likelihood of foreground star contamination increases dramatically for objects at low Galactic latitudes. Our formal criterion was to select clusters at  $|b| \gtrsim 20^\circ$  from the whole sky.

A histogram of the SCII redshift distribution is presented in Figure 3. The range of redshifts runs from 5000 to 25,000 km s<sup>-1</sup>, with fully 90% of the clusters lying between 7000 and 19,000 km s<sup>-1</sup>. The average CMB redshift of the SCII clusters is 12,050 km s<sup>-1</sup> when clusters are weighted according to the square root of the number of T-F measurements available. It is evident from Figure 3 that our sample’s distance range provides an opportunity to effectively test claims of bulk flow motions on scales of  $100 h^{-1}$  Mpc.

## 2.3. Galaxy Selection

To determine locations of target fields to be imaged, we visually scanned the Palomar Observatory Sky Survey

<sup>3</sup> The NASA/IPAC Extragalactic Database is operated by the Jet Propulsion Laboratory, California Institute of Technology, under contract with the National Aeronautics and Space Administration.

TABLE 1  
THE SCII CLUSTER SAMPLE

Cluster (1)	R.A. (B1950.0) (2)	Decl. (B1950.0) (3)	( <i>l</i> , <i>b</i> ) (deg) (4)	$c z_{\text{helio}}$ (km s <sup>-1</sup> ) (5)	$c z_{\text{CMB}}$ (km s <sup>-1</sup> ) (6)	$N_z$ (7)	<i>R</i> (8)	B-M (9)
A2806	00 37 54	-56 26 00	(306, -61)	8019 (080)	7867	27	0	I-II
A114	00 51 12	-21 58 00	(128, -85)	17436 (143)	17144	41	0	...
A119	00 53 48	-01 32 00	(126, -64)	13470 (085)	13141	73	1	II-III
A2877	01 07 36	-46 10 00	(293, -71)	7165 (058)	6974	130	0	I
A2877b	01 07 36	-46 10 00	(293, -71)	9231 (048)	9040	37	...	...
A160	01 10 12	+15 15 00	(131, -47)	12390 (141)	12072	32	0	III
A168	01 12 36	-00 01 00	(136, -62)	13365 (058)	13049	67	2	II-III:
A194	01 23 00	-01 46 00	(142, -63)	5342 (037)	5037	123	0	II
A260	01 49 00	+32 55 00	(137, -28)	10924 (111)	10664	45	1	II
A397	02 54 12	+15 45 00	(162, -37)	9803 (078)	9594	42	0	III
A3193	03 56 54	-52 29 00	(262, -47)	10559 (112)	10522	32	0	I
A3266	04 30 30	-61 35 00	(272, -40)	17775 (061)	17782	328	2	I-II
A496	04 31 18	-13 21 00	(210, -36)	9860 (059)	9809	148	1	I:
A3381	06 08 06	-33 35 00	(240, -23)	11410 (048)	11510	41	1	I
A3407	07 03 42	-49 00 00	(259, -18)	12714 (136)	12861	14	1	I
A569	07 05 24	+48 42 00	(169, +23)	5927 (043)	6011	55	0	II:
A634	08 10 30	+58 12 00	(159, +34)	7822 (042)	7922	51	0	III
A671	08 25 24	+30 35 00	(193, +33)	15092 (194)	15307	26	0	II-III:
A754	09 06 24	-09 26 00	(239, +25)	16282 (082)	16599	90	2	I-II:
A779	09 16 48	+33 59 00	(191, +44)	6967 (101)	7211	50	0	I-II:
A957	10 11 24	-00 40 00	(243, +43)	13464 (120)	13819	43	1	I-II:
A1139	10 55 30	+01 46 00	(251, +53)	11851 (071)	12216	26	0	III
A1177	11 06 48	+21 58 00	(221, +66)	9755 (081)	10079	8	0	I
A1213	11 13 48	+29 32 00	(202, +69)	14006 (090)	14304	36	1	III
A1228	11 18 48	+34 36 00	(187, +69)	10517 (034)	10794	41	1	II-III
A1314	11 32 06	+49 19 00	(152, +64)	9764 (154)	9970	28	0	III
A3528	12 51 36	-28 45 00	(304, +34)	16459 (139)	16770	30	1	II
A1736	13 24 06	-26 51 00	(313, +35)	10397 (050)	10690	62	0	III
A1736b	13 24 06	-26 51 00	(313, +35)	13724 (084)	14017	116	...	...
A3558	13 25 06	-31 14 00	(312, +31)	14342 (044)	14626	482	4	I
A3566	13 36 06	-35 18 00	(314, +26)	15370 (087)	15636	32	2	II
A3581	14 04 36	-26 47 00	(323, +33)	6865 (126)	7122	31	0	I
A1983b	14 47 24	+17 06 00	(019, +61)	11332 (062)	11524	27	...	...
A1983	14 50 24	+16 57 00	(019, +60)	13527 (045)	13715	88	1	III:
A2022	15 02 12	+28 37 00	(043, +61)	17262 (072)	17412	24	1	III
A2040	15 10 18	+07 37 00	(009, +51)	13440 (061)	13616	37	1	III
A2063	15 20 36	+08 49 00	(013, +50)	10445 (053)	10605	125	1	II:
A2147	16 00 00	+16 02 00	(029, +44)	10493 (085)	10588	93	1	III
A2151	16 03 00	+17 53 00	(032, +45)	11005 (059)	11093	143	2	III
A2256	17 06 36	+78 47 00	(111, +32)	17442 (132)	17401	94	2	II-III:
A2295b	17 59 00	+69 16 00	(100, +30)	18701 (082)	18633	6	...	...
A2295	18 00 18	+69 13 00	(099, +30)	24622 (199)	24554	9	0	II-III
A3656	19 57 12	-38 40 00	(002, -29)	5750 (064)	5586	31	0	I-II
A3667	20 08 30	-56 58 00	(341, -33)	16582 (094)	16477	128	2	I-II
A3716	20 47 54	-52 54 00	(346, -39)	13763 (064)	13618	174	1	I-II:
A3744	21 04 18	-25 41 00	(021, -40)	11386 (089)	11123	42	1	II-III
A2457	22 33 12	+01 13 00	(069, -47)	17643 (110)	17280	20	1	I-II:
A2572	23 15 54	+18 28 00	(094, -39)	11857 (100)	11495	38	0	III
A2589	23 21 30	+16 33 00	(095, -41)	12288 (095)	11925	58	0	I
A2593	23 22 00	+14 22 00	(093, -43)	12414 (086)	12049	67	0	II
A2657	23 42 18	+08 52 00	(097, -50)	12028 (137)	11662	40	1	III
A4038	23 45 06	-28 25 00	(025, -76)	9012 (063)	8713	180	2	III

NOTE.—Units of right ascension are hours, minutes, and seconds, and units of declination are degrees, arcminutes, and arcseconds.

plates for regions in the clusters containing promising disk systems appropriate for T-F work. The selection of target galaxies for this study stemmed directly from the images obtained. A discussion of the imaging for this project is contained in Papers I, II, and IV. Each image in clusters chosen for spectroscopy was searched for spiral disks with the following properties:

1. Disk inclinations  $\geq 40^\circ$ ;
2. Lack of dominating bulges—bulgy disk systems tend to be gas deficient and thus undesirable for emission-line spectroscopy, and moreover, morphological homogeneity is preferable, to limit the effects of morphological bias (§ 3.3.5);
3. No apparent warps/interacting neighbors; and

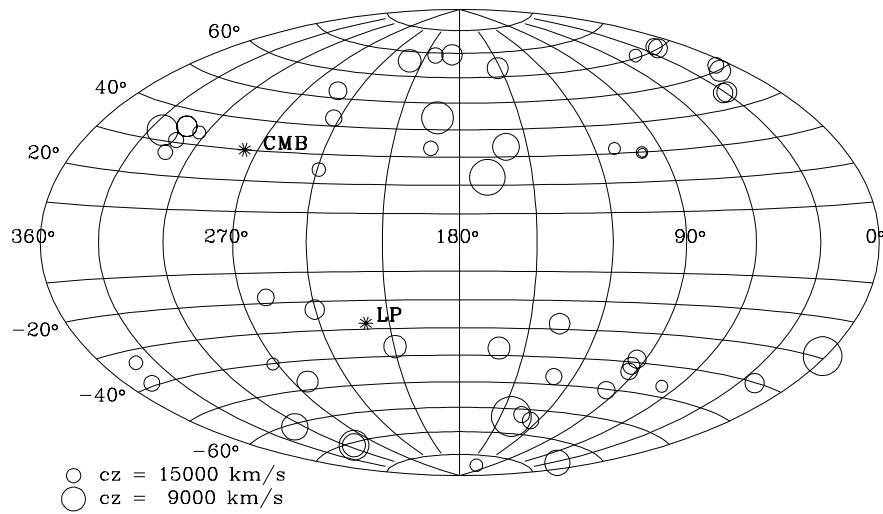


FIG. 1.—All-sky distribution of the SCII sample in Galactic coordinates. The circles are drawn inversely proportional to the cluster redshifts. The two examples in the lower left give the scale. Asterisks mark the apices of the motion of the Local Group with respect to the CMB and the LP cluster inertial frame.

4. No nearby bright stars that may affect flux measurements. It should be noted that the above properties served as guidelines for selecting T-F candidates, but occasionally the guidelines were not strictly followed, as occasionally our hand was forced by the vagaries of telescope allocations and weather conditions. Coordinates and position angles for approximately 2250 T-F candidates were obtained from the

Digitized Sky Survey<sup>4</sup> and are accurate to better than 2". The full list is available from D. A. D. upon request.

A T-F display of the collective raw data can be seen in Figure 4. The term "raw" implies that the absolute magni-

<sup>4</sup> The Digitized Sky Surveys were produced at the Space Telescope Institute under US government grant NAGW-2166. The images of these surveys are based on photographic data obtained using the Oschin Schmidt Telescope on Palomar Mountain and the UK Schmidt Telescope.

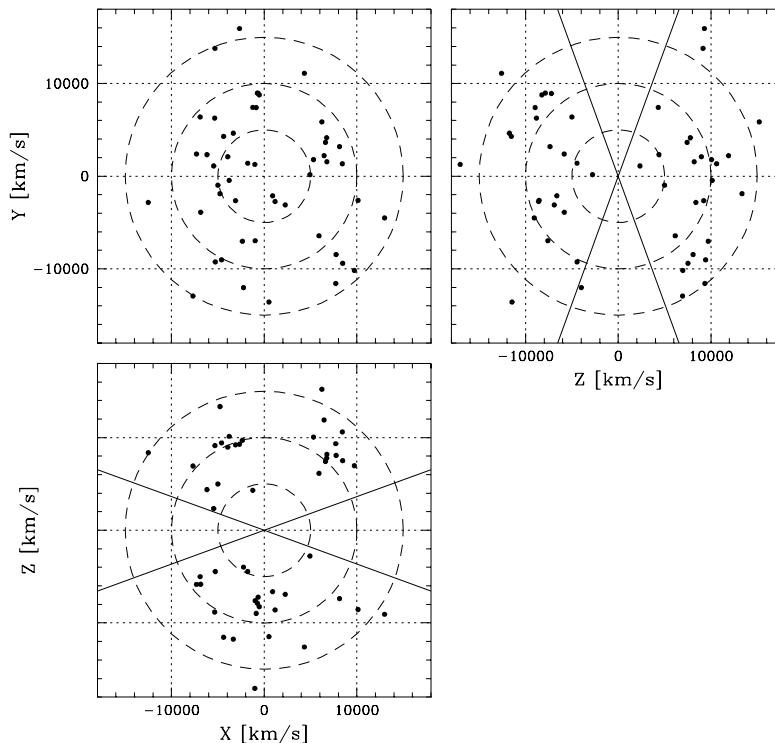


FIG. 2.—Stereographic representation in Galactic Cartesian coordinates of the 52 clusters of galaxies that make up the SCII sample. The dashed circles have radii of 5000, 10,000, and 15,000 km s<sup>-1</sup>. The solid lines in the (X, Z) and (Z, Y) plots indicate  $|b| = 20^\circ$ , the approximate extent of the zone of avoidance.

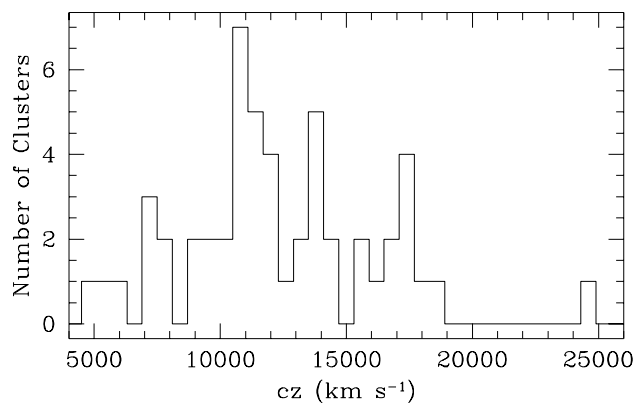


FIG. 3.—Redshift distribution of the clusters

tudes  $M_I$  and the rotational velocity widths  $W$  are corrected for all the effects described in Papers I and II (extinction, inclination, etc.) but the effects of cluster incompleteness bias and peculiar motion are not accounted for. Included is the template relation obtained below in § 3.4 (cf. eq. [13]). Hereafter we will use  $y = M_I - 5 \log h$  and  $x = \log W - 2.5$ .

### 3. THE TULLY-FISHER RELATION

The most widely applied methods for the determination of redshift-independent distances of galaxies rely on the combination of photometric (distance dependent) and kinematic (distance independent) parameters. Among them, and arguably the most accurate, are the T-F and fundamental-plane relations, used for spiral and elliptical galaxies,

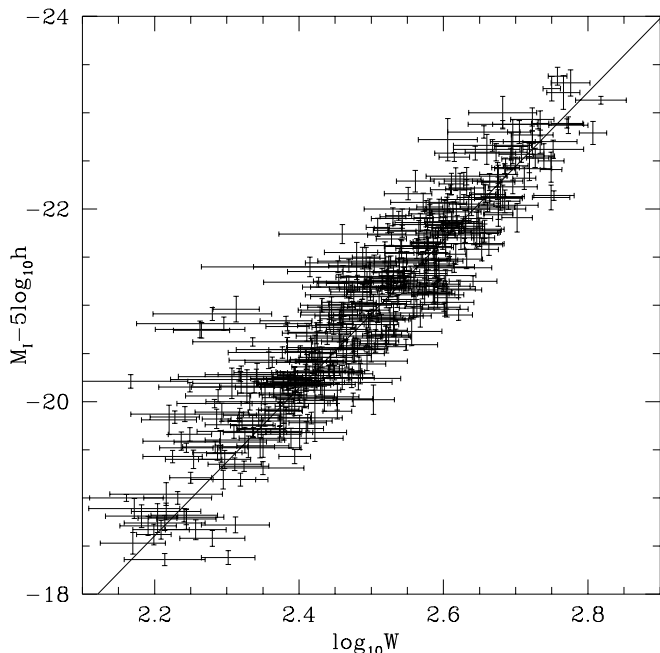


FIG. 4.—The T-F data for all galaxies. We emphasize that the data have not yet been corrected for individual cluster peculiar motion and incompleteness bias. The solid line is the template relation derived in § 3.4.

respectively. With both these methods, distances for individual galaxies, and, therefore, peculiar velocities, are computed by comparison with a fiducial *template* relation, which must be observationally derived. The template relation defines the rest reference frame, against which peculiar velocities are to be measured. The importance of accurately calibrating such a tool cannot be overemphasized. It is possible that the discrepancies between different claims of bulk motions may be partly related to insufficiently well determined template relations.

Ideally, the template employed is tied to a kinematic rest frame. In practice, the template originates from data within the sampled volume itself. We outline here our approach to calibrate the T-F relation using our sample of data from 52 rich Abell clusters distributed throughout the sky. As we shall see, the T-F zero point is obtained through an iterative process: the computation of the cluster incompleteness bias requires prior knowledge of the T-F template zero point, while the computation of the zero point demands a correction for the cluster incompleteness bias. The process does converge, however, in a small number of iterations.

#### 3.1. Calibration of the Tully-Fisher Relation

For an assumed linear T-F relation we need to determine two main parameters: a slope and a magnitude offset, or zero point. The slope of the T-F relation is best determined by a sample that maximizes the dynamic range in  $(M, \log W)$ , i.e., one that preferentially includes nearby objects. On the other hand, the magnitude zero point of the relation is best obtained from a sample of distant objects for which a peculiar motion of given amplitude translates into a small magnitude shift. An often-adopted practice to calibrate the T-F relation uses one relatively distant cluster of galaxies, for example, the rich Coma Cluster at  $cz \sim 7200 \text{ km s}^{-1}$ . Such a choice relies on the assumption that galaxies within a cluster are essentially at the same redshift—any differences in their radial velocities are attributed to the cluster's virial stretch. Thus, they all equally participate in the local peculiar velocity field and they should all obey the same local T-F relation. Another reason to choose a cluster like Coma for calibration is that, as mentioned above, the selection of a distant object limits the impact of the object's peculiar velocity  $V$ , at least to the extent that the physical size of the cluster is small in comparison with its mean distance; peculiar velocities introduce relative distortions of redshifts that are larger for nearby objects than for distant ones. In terms of magnitude, if  $V_{\text{pec}} \ll cz$ , the zero point will be off by  $\Delta m \simeq -2.17 V_{\text{pec}}/cz \text{ mag}$  (cf. eq. [14]).

There are several problems with the above calibration scheme. First, a “template” cluster needs to have a large sample of spiral galaxies. Second, even for a cluster as distant as Coma, typical cosmic velocities may bias the relation's zero point. If the cluster were moving at a plausible speed of  $500 \text{ km s}^{-1}$ , then all other estimates of peculiar velocities that use the template will systematically be off by  $500(cz/cz_{\text{template}})$ , regardless of statistical uncertainties.

To avoid such systematics in the T-F relation, G97a and G97b use a “basket of clusters” approach. Their template is derived through an iterative procedure that simultaneously determines the T-F zero point and the cluster motions of their sample. They assume that the mean peculiar velocity of the clusters farther than  $cz = 4000 \text{ km s}^{-1}$  is null, i.e.,

they zero the monopole of the more distant cluster peculiar velocity distribution function. This approach does not, however, affect the value of the dipole or higher moments and thus still allows an effective measure of possible bulk flows. The proximity of the SCI sample provides the stretch in galactic properties necessary to determine accurately the T-F slope (it is for this reason that we adopt the slope computed in G97a). Also, the large database afforded by the SCI allows the statistical uncertainty of the magnitude zero point to be reduced to 0.02–0.03 mag. The systematic uncertainty in the zero point is larger. For a sample of  $N$  objects with an rms velocity of  $\langle V^2 \rangle^{1/2}$  at a mean redshift of  $\langle cz \rangle$ , the expected accuracy of the zero point is limited by systematic concerns to

$$\sigma_a \approx \frac{2.17 \langle V^2 \rangle^{1/2}}{\langle cz \rangle \sqrt{N}} \text{ mag} . \quad (2)$$

G97a conclude the SCI systematics only allow the universal T-F zero point to be determined to within 0.04 mag. Thus the overall zero-point accuracy obtainable from the SCI sample is  $\sim 0.05$  mag. We adopt the procedure described in G97a to calibrate the T-F zero point using the SCII sample. The resulting improvement in its calibration is discussed in § 3.4.

### 3.2. Scatter of the Tully-Fisher Relation

Any relation involving observed parameters has a limited accuracy described by the amplitude of the relation's scatter. Claims of the scatter in the T-F relation vary from as low as 0.10 mag (Bernstein et al. 1994) to as high as 0.7 mag (Sandage 1994a, 1994b; Sandage, Tammann, & Feder-spiel 1995; Marinoni et al. 1998). The amplitude of the scatter does depend on wavelength, and studies in the  $I$  band typically yield the tightest relations. The efforts with the largest samples yield  $1 \sigma$  dispersion values of  $\sim 0.3$ – $0.4$  mag (Mathewson et al. 1992; Willick et al. 1995; G97a). Uncertainties in observational measurements are not the only factors that lead to the overall spread in the data. The corrections to the observed fluxes and disk rotational velocities described in Papers I and II are not exactly known, nor are the methods we detail later to account for inherent sample biases such as cluster incompleteness. Moreover, there is an *intrinsic* component to the T-F dispersion since individual galaxies have diverse formation histories. In fact, Eisenstein & Loeb (1996) advocate an intrinsic scatter of 0.3 mag, a number greater than most estimates from observational work. In light of this fact, they make the interesting claim that either spirals formed quite early or that there must be a type of feedback loop that promotes galactic assimilation.

As already established in G97a and Willick (1999), Figure 5 reinforces the notion of low intrinsic scatter. The two dotted lines indicate the velocity width and magnitude uncertainties  $\epsilon_x$  and  $\epsilon_y$ , with  $\epsilon_x$  multiplied by the T-F slope  $b$  to put it on a magnitude scale; the solid line labeled  $\epsilon_m$  =  $[(b\epsilon_x)^2 + \epsilon_y^2]^{1/2}$  represents the average measurement uncertainty. The data displayed in Figure 5 are generated using equal numbers of galaxies per data point. The circles plotted represent the average standard deviations of the residuals from the fiducial T-F relation. We see that the velocity width errors dominate those from the  $I$ -band fluxes, which are approximately independent of velocity width. Furthermore, the logarithmic velocity widths

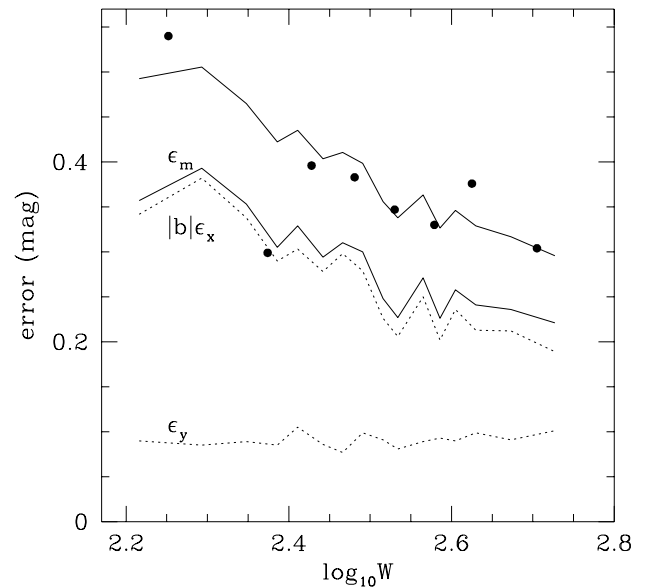


FIG. 5.—Observed scatter in the T-F relation. Running averages (in units of magnitudes) of the observed errors are given as dotted lines. The lower solid line is the sum in quadrature of the two dotted lines and represents the total measurement uncertainty. The circles indicate the standard deviations of residuals from the template T-F relation. The upper solid line is the total scatter in the T-F relation and has been computed by a sum in quadrature of the observed error distribution and an intrinsic component equivalent to that found in G97a (see eq. [4]).

become increasingly uncertain for slower rotators (cf. G97a; Willick et al. 1997). We approximate the total observed scatter with a simple linear relation that depends on the velocity width:

$$\sigma_{\text{tot}} = -0.40x + 0.38 \text{ mag} . \quad (3)$$

The total scatter found here is in general larger than that found in G97a ( $\sigma_{\text{tot}} = -0.32x + 0.32$ ). This is unsurprising given our use of optical rotation curves instead of 21 cm profiles, a comparatively easier source from which to estimate velocity widths, and since the nearer SCI galaxies generally have better determined disk inclinations. The gap between the observed scatter and the measured errors is attributed to an intrinsic scatter contribution: the top line is a sum in quadrature of our observed measurement errors,  $\epsilon_m$ , and the intrinsic scatter found in G97a:

$$\sigma_{\text{int}} = -0.28x + 0.26 \text{ mag} . \quad (4)$$

Simply put, our findings for an intrinsic component of the T-F relation agree with those of Giovanelli and Willick and their collaborators.

### 3.3. Observational Biases

#### 3.3.1. Cluster Population Incompleteness

Quite possibly the most important selection effect to consider for this observing program is that of cluster incompleteness, the preferential sampling of the bright end of the luminosity function (LF). Several authors have cautioned that cluster incompleteness can significantly alter inferred distances to clusters, though this ultimately depends on the amplitude of the scatter in the T-F relation (see G97a; Willick 1994; Sandage et al. 1995; review by Teerikorpi 1997). Schechter (1980) first advanced the notion that the repercussions of this selection effect can be circumvented

through an inverse fitting procedure, whereby the roles of the ordinate and abscissa in the T-F diagram are reversed. The argument goes as follows: if there are no observational effects working against the selection of velocity widths and if the errors on the absolute magnitudes are negligible, then a fit to  $\log W$  versus  $M$  will not be affected by a cutoff at faint magnitudes. Unfortunately, magnitude errors cannot be ignored (see Fig. 5), and moreover, the errors in  $M$  and  $\log W$  are coupled through inclination corrections; T-F data do not obey a sharp faint magnitude limit. Inevitably, the absence of faint galaxies in a T-F sample artificially brightens the zero point and lowers the slope. We describe next our methodology to account for the effect.

Our first concern is to quantify the characteristics of the observed luminosity distribution with respect to the actual LF. As an aside, we note that current work by Andreon (1998) supports the notion of a canonical spiral LF by proposing that the LF for the separate morphological classes E, S0, and S is independent of environment—observed differences in the overall LF for different environments are merely due to varying proportions of the morphological classes (but see Iovino et al. 1993). Our first step is to sum up the observed luminosities in bins of absolute magnitude. Computing such absolute magnitude histograms for each individual cluster, where the membership counts can be as small as  $\sim 5$ , would not be statistically indicative on the whole. We therefore compute *average* histograms for several distance ranges of width  $2000 \text{ km s}^{-1}$ . We define the completeness function as the ratio of the observed luminosity distribution to the assumed intrinsic luminosity distribution. The following figures have been constructed assuming a Schechter LF with  $M^* = -21.6$  and  $\alpha = -0.5$  (see Fig. 20 of Paper IV), but final T-F templates using

other Schechter parameters will also be provided. Figure 6 displays a smoothed representation of the completeness functions, along with our fitted approximation. As in G97a, we borrow a relation from Fermi-Dirac statistics to model completeness:

$$c(y) = \frac{1}{e^{(y-y_t)/\beta} + 1}, \quad (5)$$

where  $y_t$  represents a transition luminosity in the fit and  $\beta$  characterizes the steepness of the drop. It should be noted that the final T-F template is rather robust in terms of the completeness function construction. The template is largely insensitive to the choice of distance regimes, variations in the Fermi-Dirac fit profile, and the luminosity bin widths. Reasonable alterations in these parameters induce negligible changes in the T-F template zero point. With the estimation of the completeness function in hand, we can now quantify a given cluster's incompleteness bias via Monte Carlo simulations.

### 3.3.2. Monte Carlo Simulations of Cluster Parent Samples

Our task is simplified by assuming the bias-corrected slope derived in G97a is valid for our sample, a justifiable assumption given the relative propinquity of their data—a broader dynamic range can be more easily sampled in nearby clusters. Furthermore, least-squares fits to the data yield slopes that, within the errors, agree with the T-F slope from G97a. On a more qualitative level, inspection of Figure 4 indicates that our data agree with the slope from G97a. It is thus sufficient to only determine the bias in the T-F offset for each cluster.

We compute the bias as follows: For each galaxy a large number ( $N_{\text{iter}} = 10^3$ ) of trial T-F data points are generated

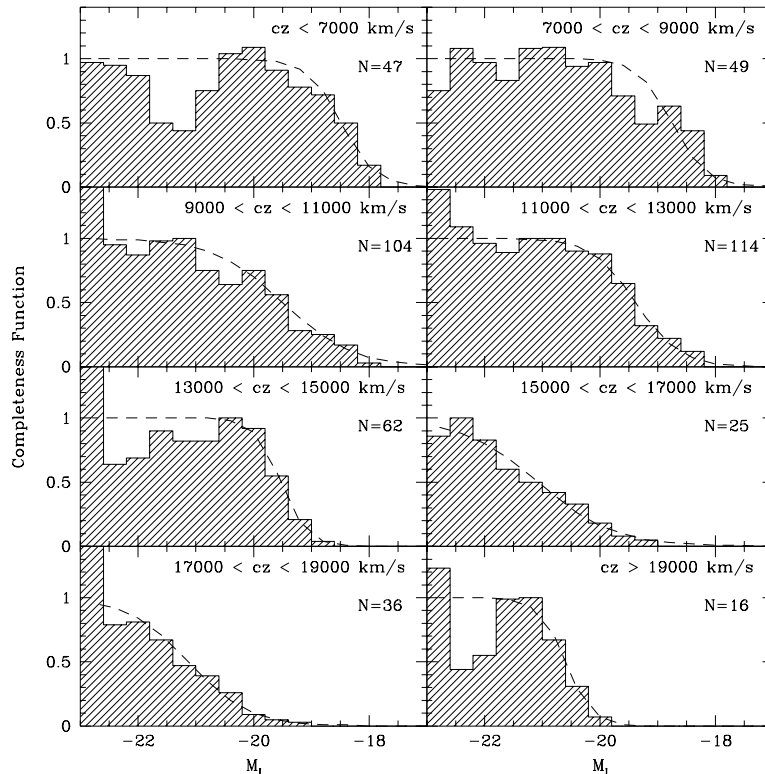


FIG. 6.—Distributions of cluster completeness for separate distance ranges. The dashed lines are our smoothed approximation to the completeness function. The number of galaxies within each redshift range is indicated.



that mimic the general characteristics of the actual data. Within each trial, a random (Gaussian deviate) magnitude offset  $\Delta y_{\text{trial}}$  is first chosen according to the T-F scatter relation, equation (3), which depends on the galaxy's measured velocity width parameter  $x$ . The addition of this offset to the magnitude inferred from the final, template T-F relation yields the trial absolute magnitude:

$$y_{\text{trial}} = b_{\text{TF}} x + a_{\text{TF}} + \Delta y_{\text{trial}}. \quad (6)$$

The trial magnitude is kept only if it is a likely magnitude, i.e., a second random number from the interval  $[0, 1]$  must be less than  $c(y_{\text{trial}})$ , the completeness value for the trial luminosity. Otherwise, the process is repeated until a likely magnitude is found. After all  $N_{\text{iter}}$  iterations are complete for a given galaxy, the incompleteness bias is taken to be the mean difference between the trial luminosities and that expected from the T-F relation, i.e.,

$$-\Delta y_{\text{icb}} = \frac{\sum_i^{N_{\text{iter}}} y_{\text{trial},i}}{N_{\text{iter}}} - (b_{\text{TF}} x + a_{\text{TF}}). \quad (7)$$

Figure 7 gives the biases calculated as a function of velocity width and the polynomials we fitted to them. The general property of the computed bias is as expected: incompleteness biases “turn on” at higher velocity widths for more distant objects. An incompleteness bias-corrected zero point for each cluster is then extracted from the cluster's distribution of observed velocity widths and bias-corrected absolute magnitudes. A tabulation of the offsets from the template zero point,  $a - a_{\text{TF}}$ , is provided in Table 2. The cluster names are listed first and are followed by the number of cluster members  $N_{\text{TF}}$  with reliable photometry and velocity widths. The next two columns are measures of the cluster offsets from the template zero point, the second of which is

corrected for the effect of cluster incompleteness and includes an indication of its uncertainty  $\epsilon_a$  in parentheses, e.g.,  $-0.06$  (10) implies  $-0.06 \pm 0.10$  mag. The last column of data listed is  $\sigma_a$ , the dispersion in the difference between the template and the cluster's set of absolute magnitudes. It is used to compute the offset uncertainty:

$$\epsilon_a = \sigma_{\text{max}} / \sqrt{N_{\text{TF}}}, \quad (8)$$

where  $\sigma_{\text{max}}$  is taken to be the maximum of  $\{0.35 \text{ mag}, \sigma_a\}$  to avoid overly optimistic measures of offset uncertainty in cases of chance alignment of the data due to small number statistics. Last, we remark that the proper incorporation of selection effect corrections is vital to determining the T-F template, but the exact evaluation of such biases necessarily requires a T-F template. A stable solution to this circular process is found within a few iterations.

### 3.3.3. Homogeneous Malmquist Bias

An observational bias commonly referred to as the “homogeneous Malmquist bias” is a distance underestimate for a galaxy drawn from a uniform distribution of galaxies. The bias is a direct result of the error on the measured distance—a galaxy taken from a Poissonian spatial distribution and measured to be at a distance modulus  $\mu_m \pm \Delta\mu$  is more likely to actually lie between  $\mu_m$  and  $\mu_m + \Delta\mu$  than in the range from  $\mu_m$  to  $\mu_m - \Delta\mu$ , as a result of the larger volume of the more distant shell. Following the reasoning given in Lynden-Bell et al. (1988), it can be shown that a measured distance  $R_m$  is, on average, an underrepresentation of the true distance by the factor  $\exp 3.5\Delta^2$ :

$$V = cz - H_0 R_m \rightarrow cz - H_0 R_m e^{3.5\Delta^2}. \quad (9)$$

The factor  $\Delta = 10^{0.2\epsilon_a} - 1$  is the fractional error in the T-F distance measurement, roughly 17% for individual galaxies

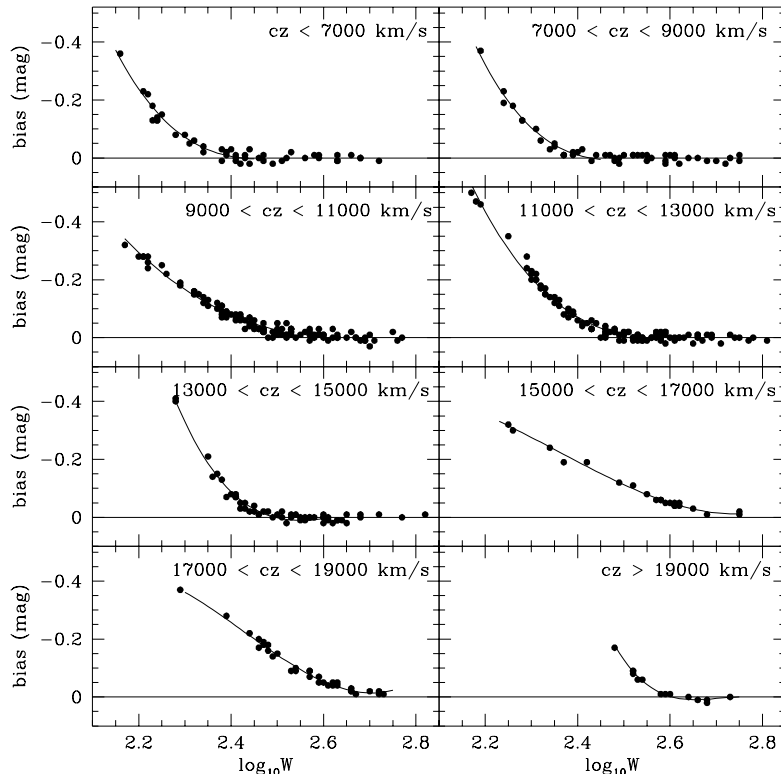


FIG. 7.—Incompleteness bias as a function of rotational velocity width. Individual points are the biases generated for each galaxy from Monte Carlo simulations, and the solid lines are polynomial fits to the bias.

TABLE 2  
CLUSTER OFFSETS

Cluster	$N_{TF}$	$a_{bias} - a_{TF}$	$a - a_{TF}$	$\sigma_a$	Cluster	$N_{TF}$	$a_{bias} - a_{TF}$	$a - a_{TF}$	$\sigma_a$
A2806 .....	10	-0.15	-0.13 (11)	0.27	A3528 .....	3	0.03	0.18 (07)	0.12
A114 .....	9	-0.01	0.07 (14)	0.41	A1736 .....	6	-0.03	0.01 (18)	0.44
A119 .....	6	0.04	0.05 (16)	0.38	A1736b .....	4	-0.03	-0.03 (18)	0.32
A2877 .....	7	-0.01	0.03 (15)	0.40	A3558 .....	8	-0.13	-0.10 (15)	0.43
A2877b .....	5	-0.10	-0.08 (16)	0.14	A3566 .....	9	-0.13	-0.03 (12)	0.23
A160 .....	6	-0.06	-0.05 (18)	0.45	A3581 .....	4	-0.01	0.04 (20)	0.40
A168 .....	9	-0.13	-0.12 (13)	0.38	A1983b .....	8	-0.27	-0.26 (12)	0.25
A194 .....	13	0.05	0.09 (13)	0.45	A1983 .....	7	-0.14	-0.07 (19)	0.50
A260 .....	9	0.13	0.23 (14)	0.42	A2022 .....	8	0.06	0.14 (12)	0.32
A397 .....	14	-0.17	-0.13 (15)	0.57	A2040 .....	10	-0.10	-0.03 (14)	0.43
A3193 .....	6	-0.14	-0.10 (14)	0.09	A2063 .....	18	-0.18	-0.14 (09)	0.36
A3266 .....	2	0.12	0.31 (25)	0.21	A2147 .....	19	-0.09	-0.06 (09)	0.39
A496 .....	9	-0.18	-0.13 (12)	0.36	A2151 .....	22	-0.08	-0.06 (08)	0.40
A3381 .....	4	-0.17	-0.16 (18)	0.12	A2256 .....	8	-0.04	-0.01 (12)	0.33
A3407 .....	8	-0.07	0.03 (21)	0.58	A2295b .....	4	-0.05	0.05 (18)	0.36
A569 .....	13	0.02	0.06 (10)	0.30	A2295 .....	10	0.07	0.10 (12)	0.39
A634 .....	8	0.04	0.06 (12)	0.35	A3656 .....	6	0.01	0.03 (14)	0.28
A671 .....	9	-0.05	0.02 (12)	0.34	A3667 .....	4	0.27	0.37 (18)	0.28
A754 .....	3	-0.07	0.01 (42)	0.73	A3716 .....	14	-0.08	-0.06 (09)	0.22
A779 .....	14	0.01	0.03 (09)	0.27	A3744 .....	11	-0.03	0.03 (11)	0.37
A957 .....	6	0.08	0.13 (14)	0.16	A2457 .....	9	-0.02	0.02 (12)	0.32
A1139 .....	11	-0.17	-0.13 (12)	0.39	A2572 .....	5	-0.11	-0.08 (16)	0.13
A1177 .....	6	-0.11	-0.01 (15)	0.37	A2589 .....	6	-0.03	0.04 (14)	0.23
A1213 .....	6	-0.12	-0.12 (14)	0.33	A2593 .....	12	0.09	0.13 (10)	0.30
A1228 .....	13	0.04	0.12 (10)	0.33	A2657 .....	5	-0.03	-0.01 (16)	0.26
A1314 .....	8	-0.04	0.03 (12)	0.31	A4038 .....	7	-0.06	-0.02 (13)	0.35

and 6% for our clusters. It was shown in G97a that such a correction for clusters of galaxies is rather small, almost to the point of being negligible (of order 1% on individual cluster distances). The inclusion of the above correction factor in later computations in this work does not change results appreciably. The influence of the homogeneous Malmquist bias on the inferred local bulk flow is discussed in Paper III.

The Abell/ACO clusters do not represent a homogeneously distributed population. Thus, the application of a homogeneous Malmquist bias correction may appear incorrect. However, a correction that takes into account the clustering properties of clusters differs from the homogeneous Malmquist bias correction only in the second order. Given the minuscule size of the correction and the uncertainty of a possible ‘‘inhomogeneous’’ Malmquist bias correction, we consider the application of a homogeneous Malmquist bias correction a satisfactory approach.

### 3.3.4. Cluster Size

In calculating absolute magnitudes, we assume that each cluster member within 1 Abell radius of the cluster center is at a distance equal to the average of all the redshifts available for the cluster from the literature. It is unlikely that a given galaxy will actually be at this distance, but it is a useful approximation if the distance to the cluster is significantly larger than the cluster’s virial size. For all but a handful of our clusters this is the case, so cluster size biases play a small role in our analysis.

Our concern here is the method of averaging used. The calculation of a cluster offset involves averaging over absolute magnitudes. Thus, averages of the logarithms of the distances are computed, while the logarithm of the average distance is actually desired. This results in a systematic

underestimate of cluster distances. We can use either the angular distribution on the sky of the cluster galaxies or the Abell radius to infer the approximate physical size of the each cluster. Simple analytic calculations using either estimate of the cluster size show that the amplitude of the bias is at most of order 0.001 mag for even our closest clusters, so we shall not concern ourselves with this effect any further. A more serious concern, the morphological dependence on the T-F relation, is investigated next.

### 3.3.5. Morphology

Ideally, scientific models are simple and are thus constructed with the fewest number of free parameters the data demand. In T-F work, it would be preferable to limit the range of morphologies sampled, since physical parameters are known to vary along the Hubble sequence (Roberts & Haynes 1994). For example, it has been shown that, for a given (optical) luminosity distribution, the velocity width distribution for early-type galaxies is shifted to higher rotational speeds with respect to the distribution for later types (Roberts 1978). There is evidence, however, that the T-F differences between morphological types appear to diminish at wavelengths longer than *I* band (e.g., Aaronson & Mould 1983). Regardless, we are fortunate that one sample selection criterion of ours, that of disks being rich in ionized gas, encouraged a rather homogeneous sample comprising mainly Sc types. Our sample has the following population properties: 14% are of type earlier than Sb, 16% are type Sb, and 70% are classified as Sbc or later. The majority (52%) of the galaxies are type Sc.

Our sample affords statistically significant tests of T-F morphological dependencies. We plot in Figure 8 the T-F parameters with symbols differentiated according to morphological class. Filled circles symbolize Sb types, whereas

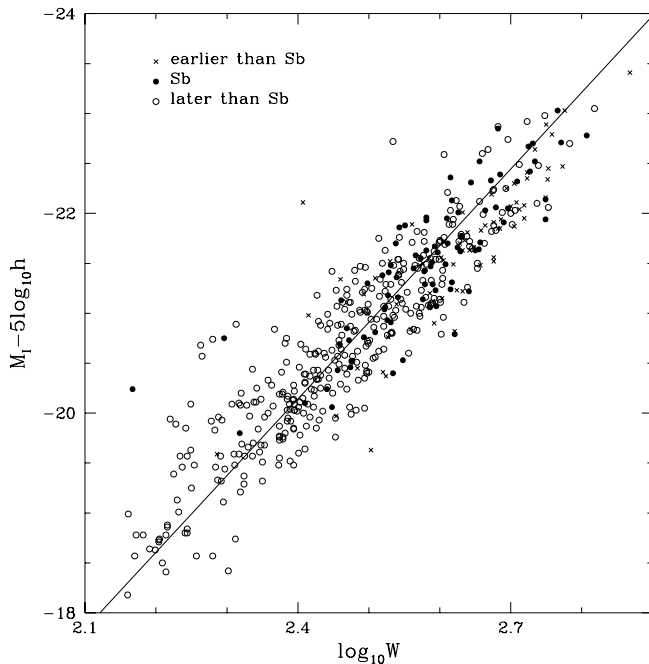


FIG. 8.—The T-F diagram differentiated according to morphological class. Crosses represent galaxies earlier than Sb, filled circles symbolize type Sb, and open circles are for Sbc and later. The data are corrected for cluster peculiar motions.

open circles and crosses represent types later and earlier than Sb, respectively. The plot includes the data for all galaxies deemed to have reliable velocity widths, with each cluster member corrected for cluster peculiar motion. The solid line shown uses the fiducial T-F slope of  $b_{TF} = -7.68$

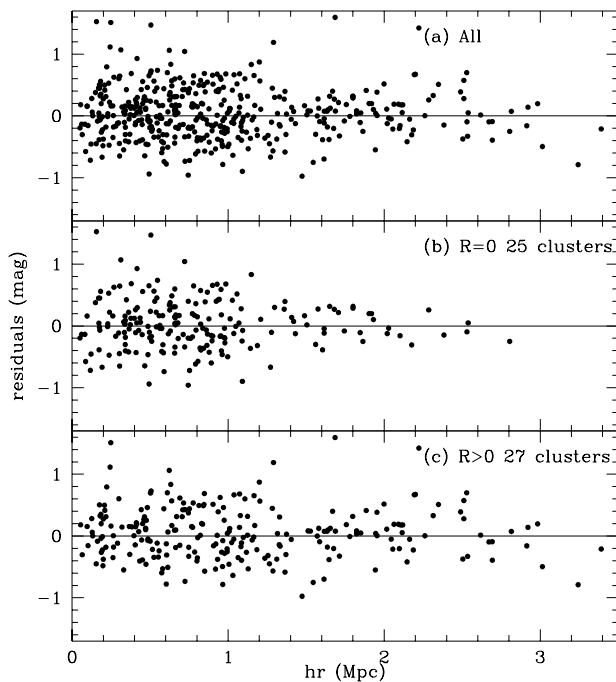


FIG. 9.—A test of environmental bias. T-F residuals are given vs. projected physical distance from the cluster center. The data are corrected for peculiar velocity and morphological offsets; (a) displays all the cluster data, whereas (b) and (c) differentiate between cluster richness.

and zero point  $a_{TF} = -20.91$  mag (cf. § 3.4). As found in G97a, a clear distinction is evident between the three Hubble types in the form of a fainter zero point for earlier types. The error-weighted averages of the offsets  $\Delta m_T$  from the template zero point for the three morphological classes differ in the following ways for our sample:

Types earlier than Sb:  $-0.27$  ( $-0.32$ ) mag;

Type Sb:  $-0.11$  ( $-0.10$ ) mag;

Other types: unchanged.

The numbers given in parentheses are those from G97a. For consistency, we will continue to utilize the offsets obtained in G97a.

### 3.3.6. Environment

Yet another possible bias in our sample is the effect of environment. For instance, the more distant clusters in our sample (and the Abell/ACO catalog in general) tend to be richer. A richer cluster typically has a stronger intracluster medium X-ray flux and a more regular, elliptical-dominated core (see, e.g., Sarazin 1986). Spiral galaxies predominantly lie in a rich cluster's periphery, and the closer a spiral disk is to the cluster center, the less likely it is to contain neutral hydrogen gas (Giovanelli & Haynes 1985). This lack of interstellar gas within clusters of galaxies may be due to evaporation into the hotter intracluster gas, or it may be attributed to "stripping" originating from either tidal galaxy-galaxy interactions or ram pressure ablation on intracluster gas. Rubin, Ford, & Whitmore (1988) and Whitmore, Forbes, & Rubin (1988) claim that the inner spiral galaxies within clusters exhibit falling rotation curves (RCs), as opposed to the asymptotically flat or rising RCs usually seen in the cluster periphery and field. Furthermore, they find that cluster RCs may be of lower amplitude than field RCs. They offer the explanation that the falling (and lower amplitude) RCs arise from mass loss—the inner galaxies have had their dark matter halos stripped—or that the cluster environment simply inhibits halo formation. A related finding by Whitmore et al. (1988) is a monotonic increase in the mass-to-light ratio, with cluster radius, which they ascribe to the changing RC shape with cluster radius. This view has been contested, however, by Amram et al. (1993) and Vogt (1995), who find little evidence for any gradients in the outer portions of RCs. If RCs in the inner regions of rich clusters do indeed differ from RCs in other environments, the ramifications are significant. The dependence of the T-F relation and/or its dispersion on environment are possible consequences. Finally, we point out that rich clusters represent high-density peaks and may thus be home to a recent merger; at least one-third of all rich clusters are home to a recent inhomogeneous superposition of two or more separate systems (Girardi et al. 1997). It is prudent to verify whether environment plays a significant role in our data.

Figure 9 displays one such test of environmental bias. For each cluster member we have plotted residuals from the T-F relation as a function of projected distance from the nominal cluster center. Figure 9a displays the data for all cluster members, while Figures 9b and 9c differentiate between Abell cluster richness. All data are corrected for peculiar velocity and morphological offsets. We see no apparent trend with projected cluster radius in any of the panels. This is in agreement with the work of Biviano et al. (1990) and G97a, which showed no change in the T-F relation for different environments. We consequently do not

TABLE 3  
TEMPLATE FIT PARAMETERS

Sample	$N$	$a$	$\epsilon_a$	$\sigma_a$	$\chi^2/\text{dof}$
No incompleteness bias .....	441	-20.96	0.02	0.39	1.1
$\alpha_{\text{LF}} = -0.50, M^* = -21.6$					
Standard .....	441	-20.91	0.02	0.38	1.1
2.5 $\sigma$ clip .....	425	-20.91	0.02	0.34	0.9
$60^\circ < i < 80^\circ$ .....	252	-20.91	0.02	0.38	1.2
$i > 45^\circ$ .....	429	-20.91	0.02	0.38	1.1
$W > 150, y < -18.5$ .....	428	-20.92	0.02	0.37	1.1
$T \leq \text{Sb}$ .....	139	-20.95	0.03	0.38	1.3
$T > \text{Sb}$ .....	302	-20.89	0.02	0.37	1.0
$cz > 10,000 \text{ km s}^{-1}$ .....	325	-20.92	0.02	0.38	1.1
$N_{\text{mem}} \geq 5$ .....	413	-20.92	0.02	0.38	1.1
$\theta_{\text{proj}} < 1$ Abell radius .....	347	-20.91	0.02	0.39	1.1
$ cz - cz_{\text{clus}}  < 1000 \text{ km s}^{-1}$ .....	368	-20.91	0.02	0.38	1.1
Including foreground and background .....	510	-20.90	0.02	0.39	1.2
$\alpha_{\text{LF}} = -0.75, M^* = -22.0$					
Standard .....	441	-20.90	0.02	0.38	1.1
2.5 $\sigma$ clip .....	425	-20.90	0.02	0.34	0.9
$60^\circ < i < 80^\circ$ .....	252	-20.90	0.02	0.38	1.2
$i > 45^\circ$ .....	429	-20.90	0.02	0.37	1.1
$W > 150, y < -18.5$ .....	427	-20.91	0.02	0.37	1.1
$T \leq \text{Sb}$ .....	139	-20.95	0.03	0.38	1.3
$T > \text{Sb}$ .....	302	-20.88	0.02	0.37	0.9
$cz > 10,000 \text{ km s}^{-1}$ .....	325	-20.91	0.02	0.38	1.1
$N_{\text{mem}} \geq 5$ .....	413	-20.91	0.02	0.34	1.1
$\theta_{\text{proj}} < 1$ Abell radius .....	347	-20.90	0.02	0.38	1.1
$ cz - cz_{\text{clus}}  < 1000 \text{ km s}^{-1}$ .....	368	-20.90	0.02	0.38	1.1
Including foreground and background .....	510	-20.89	0.02	0.39	1.2

consider environmental bias to be a serious concern with our data.

### 3.4. The Template Relation

Let  $a_k$  be the T-F zero point for cluster  $k$  and  $\Delta y_{\text{pec},k} = a_k - a_{\text{TF}}$  be the shift due to the cluster's peculiar motion. The  $i$ th cluster member's absolute magnitude can then be expressed as

$$y_i = y_{\text{cor},i} - \Delta y_{\text{icb},i} - \Delta y_{\text{pec},k}, \quad (10)$$

where  $\Delta y_{\text{icb}}$  is the cluster's incompleteness bias correction described in § 3.3.1 and  $y_{\text{cor},i} = m_{\text{cor}} - 5 \log(cz_{\text{clus}}/100) - 25$ ,  $m_{\text{cor}}$  being the corrected apparent magnitude given by equation (1) in Paper II and  $cz_{\text{clus}}$  the cluster systemic recession velocity in units of  $\text{km s}^{-1}$ . We compute the  $k$ th cluster's zero point by averaging over the individual cluster members, i.e.,

$$a_k = \frac{\sum_i^{N_k} (y_i - bx_i)/\epsilon_i^2}{\sum_i^{N_k} 1/\epsilon_i^2}, \quad \epsilon_i^2 = (\epsilon_{x,i} b)^2 + \epsilon_{y,i}^2 + \epsilon_{\text{int}}^2 \quad (11)$$

with  $N_k$  representing the number of cluster members in the  $k$ th cluster.<sup>5</sup> The uncertainty  $\epsilon_{a,k}$  of the above zero-point

computation is described by equation (8). The calculation of the template zero point  $a_{\text{TF}}$  follows. Alternative estimators of  $a_{\text{TF}}$  are

$$a_{\text{TF}} = \frac{\sum_k N_k a_k}{\sum_k N_k} \quad \text{or} \quad \frac{\sum_k a_k / \epsilon_{a,k}^2}{\sum_k 1 / \epsilon_{a,k}^2} \quad \text{or} \quad \frac{\sum_j^N (y_j - bx_j) / \epsilon_j^2}{\sum_j^N 1 / \epsilon_j^2}. \quad (12)$$

The first two estimators are averages over the individual cluster zero points, weighted either by the number of cluster members or by the cluster zero-point uncertainties. The third calculation is a simple average over all  $N$  cluster galaxies, with each galaxy weighted by its total uncertainty. The three estimators give global zero points that agree within the estimated errors (0.02 mag); we adopt the third computation. Our definition of a T-F template zero point is based on the assumption that the average peculiar velocity of the cluster set is null.

Table 3 lists results for several subsets of the data and for two different Schechter LFs:  $\alpha = -0.50$ ,  $M^* = -21.6$  and  $\alpha = -0.75$ ,  $M^* = -22.0$ . A few fit parameters are listed, including the number of galaxies used, the T-F template zero point and its associated total uncertainty (i.e., considering both statistical concerns and the kinematic uncertainty described by eq. [2]), an estimate of the scatter, and  $\chi^2$  divided by the number of degrees of freedom. Note that the dispersion and the zero-point uncertainty remain relatively unchanged across all subsets. The fact that the zero point differs slightly for late- and early-type galaxies is expected—

<sup>5</sup> Though we are only solving for the relation's offset here, this mode of calculation is similar in spirit to the bivariate calculations described in G97a, in that both magnitude and velocity width errors are considered.

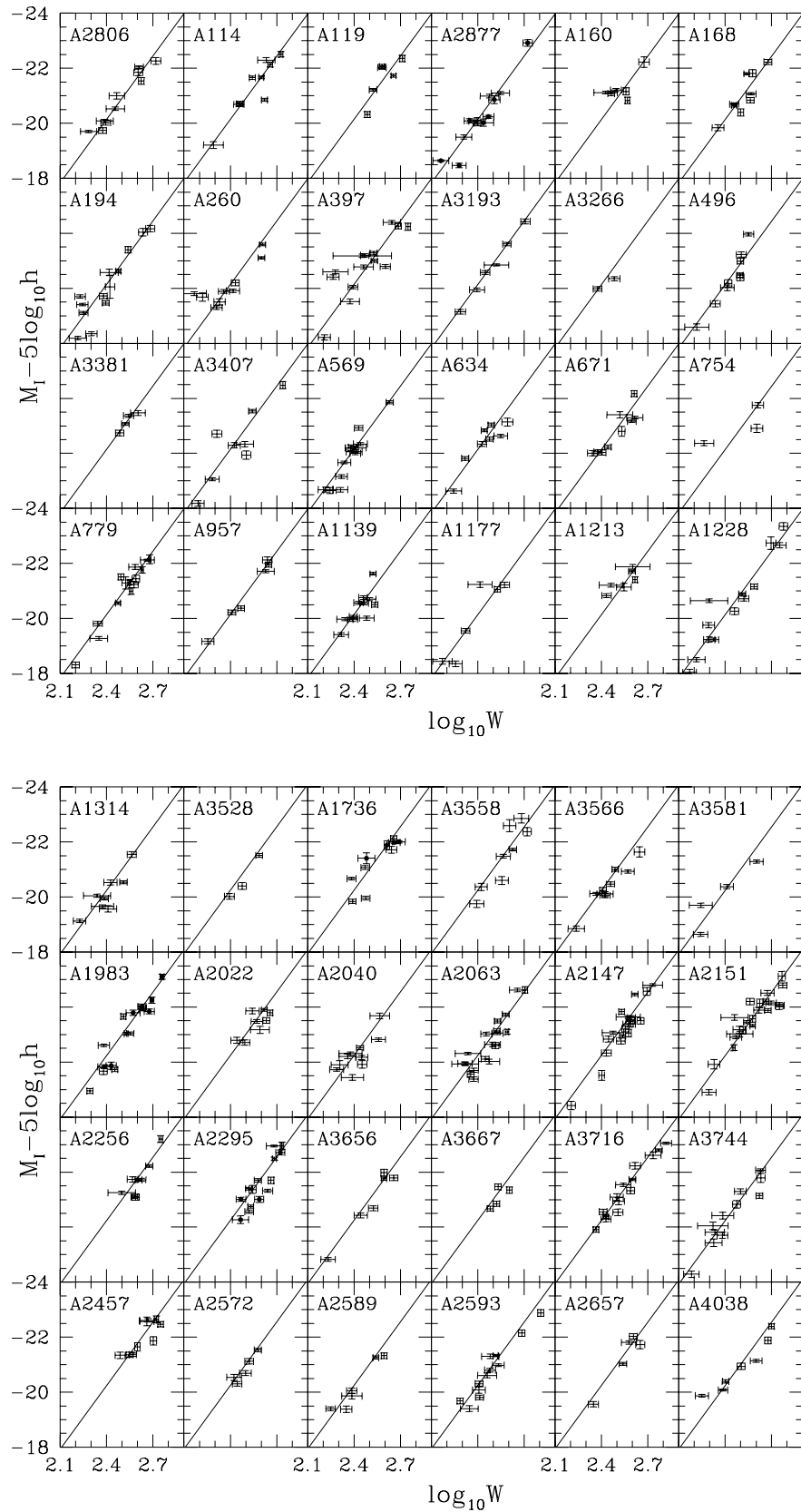


FIG. 10.—T-F plots for the clusters. Only cluster members are included in these plots. Each luminosity is corrected for cluster incompleteness and cluster peculiar velocity. The morphological offset described in § 3.3.5 for Sb and earlier-type galaxies is incorporated. The new T-F template relation is drawn as a reference (eq. [13]).

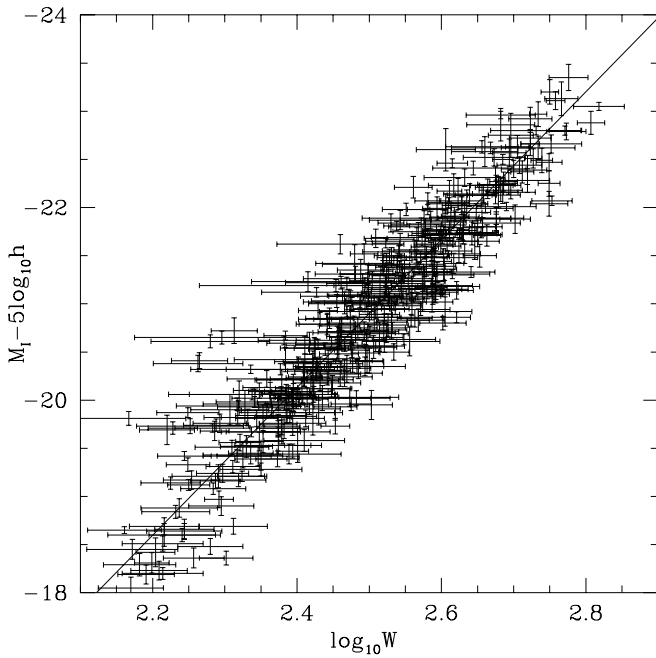


FIG. 11.—The T-F data for all galaxies, corrected for peculiar motions, incompleteness bias, and the morphological type offset described in § 3.3.5. The new T-F template relation is drawn as a reference (eq. [13]).

we saw earlier that the morphological type correction of  $-0.32$  mag advocated in G97a for Sa and Sab galaxies is possibly too large for our sample by a few hundredths of a magnitude. We should also point out that the slightly brighter zero point seen for objects beyond  $10,000 \text{ km s}^{-1}$  works against recent claims by Tammann (1999) and Zehavi et al. (1998) that the Hubble constant is higher within  $\sim 10,000 \text{ km s}^{-1}$  than it is beyond this distance. For our purposes, a fractional decrease by  $\epsilon_H$  in  $H_0$  beyond  $10,000 \text{ km s}^{-1}$  should yield a zero point that is fainter by  $5\epsilon_H \log e$ , or  $0.04$  mag for  $\epsilon_H = 0.02$ . In contrast, our data reflect a slightly brighter zero point beyond  $10,000 \text{ km s}^{-1}$ .

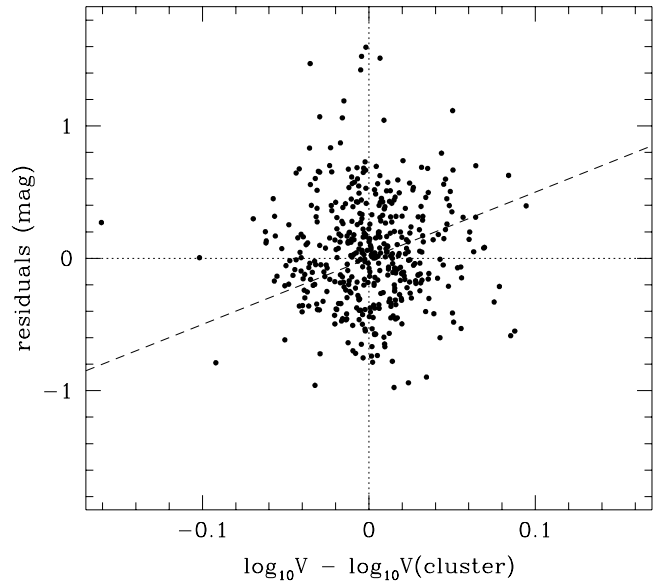


FIG. 12.—A test of cluster membership in the form of T-F residuals as a function of separation from the cluster redshift. A line of slope 5 is given, the relation on which field galaxies incorrectly assumed to be cluster members should lie.

Figure 10 gives the T-F plots for each cluster, and Figure 11 combines the data for all SCII galaxies. The data are corrected for cluster incompleteness bias and cluster peculiar motion, in accordance with equation (10). In the A2877, A1736, A1983, and A2295 panels, the error bars containing filled circles represent members of “A2877b,” “A1736b,” “A1983b,” and “A2295b,” respectively. The new T-F template is shown as well:

$$M_I - 5 \log h = -7.68(\log W - 2.5) - 20.91 \text{ mag} . \quad (13)$$

The residuals given in Figure 12 indicate the quality of the cluster membership assignments. Since the abscissa is

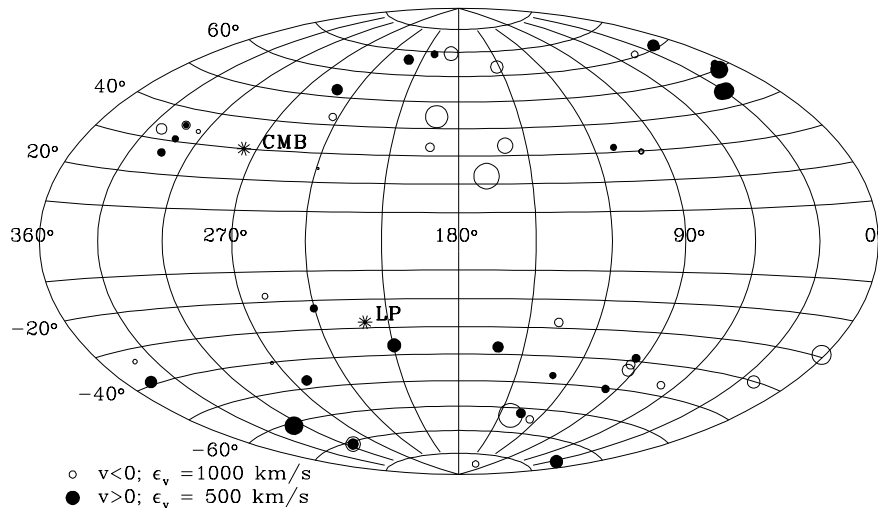


FIG. 13.—All-sky distribution of the SCII peculiar velocity sample in Galactic coordinates. The symbol diameters are inversely proportional to the peculiar velocity uncertainties. The two examples in the lower left give the scale. Filled (open) circles refer to positive (negative) peculiar velocities in the CMB frame. Asterisks mark the apices of the motion of the Local Group with respect to the CMB and the LP cluster inertial frame.

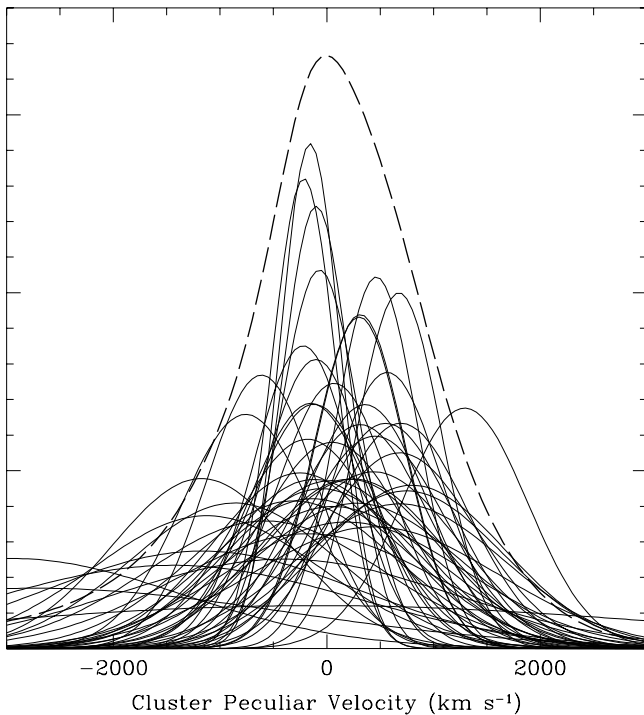


FIG. 14.—A display of equal-area Gaussians representing the peculiar velocity sample. Each Gaussian is centered at the value of a cluster peculiar velocity, has a dispersion given by the uncertainty in the peculiar velocity measurement, and has an amplitude that is inversely proportional to the uncertainty. The sum of the Gaussian profiles is given by the thick dashed line.

the difference between individual and cluster redshifts, the center of each cluster corresponds to the point (0, 0). Moreover, residuals from field galaxies that are receding according to Hubble expansion but were incorrectly declared cluster members should, on average, lie on the line of slope 5. There is no clear evidence of a significantly large subsample of improperly assigned memberships.

#### 4. THE PECULIAR VELOCITY SAMPLE

We interpret the departure of a cluster's average zero point from that of the template relation as an indication of peculiar motion, with larger departures from the template implying larger amplitude peculiar velocities. Quantitatively, for a cluster at a redshift  $z$  with an average departure from the template of  $a - a_{TF}$ , we write the peculiar velocity as

$$V = cz(1 - 10^{0.2(a - a_{TF})}). \quad (14)$$

We compute peculiar velocities and a measure of their errors for the SCII cluster sample and display the results in Table 4 and Figure 13, an Aitoff projection of Galactic coordinates. The symbols plotted in the figure reflect both the radial directions of the peculiar velocities and their uncertainties—in the CMB reference frame, open (filled) circles represent approaching (receding) clusters and the circle size is inversely proportional to the accuracy of the measurement. The largest cluster peculiar velocities, e.g., those for A3266 and A3667, are also the most uncertain, as the clusters are poorly sampled.

Our sample includes the central portions of various high-density peaks and/or superclusters in the local universe. It is

significant to note that their motions are consistent with small departures from rest in the CMB frame, within the quoted error. For instance, the Shapley supercluster, represented here by its core (A3558) and some peripheral members (A1736, A3528, and A3566), has an average CMB velocity of  $118 \pm 495 \text{ km s}^{-1}$ . The Hercules region (A2147 and A2151) and the A2572-A2589-A2593-A2657 supercluster are also slow movers, with average peculiar velocities of  $307 \pm 301$  and  $-222 \pm 372 \text{ km s}^{-1}$ , respectively. These small motions are consistent with the notion that such massive systems best represent “kinematic anchors” in the local velocity field.

#### 4.1. The One-dimensional Peculiar Velocity Distribution

It is useful to estimate the line-of-sight distribution of peculiar velocities. The amplitude of that distribution has been known to be a very sensitive discriminator of cosmological models (see, e.g., Bahcall & Oh 1996). The SCII cluster sample is relatively distant and the cluster membership counts are relatively anemic when compared with the SCI sample of G97b. Consequently, SCII peculiar velocities are much less certain and the overall distribution shown in Figure 14 is significantly broadened by measurement errors. The peculiar velocities are represented by equal-area Gaussians centered at the peculiar velocity of each cluster, with dispersions equal to the estimated peculiar velocity errors. The thick dashed line superposed on the plot is the sum of the individual Gaussians (its amplitude has been rescaled for plotting purposes). The  $1 \sigma$  dispersion in the observed distribution of peculiar velocities is found from a Gaussian fit to the dashed line:  $\sigma_{1D,obs} = 796 \text{ km s}^{-1}$ . This value, however, is biased upward by measurement errors. Recovering an estimate of the true value can easily be obtained via Monte Carlo simulations, yielding  $\sigma_{1D} = 341 \pm 93 \text{ km s}^{-1}$ , where the error estimate derives from the scatter in the dispersions of the simulated samples. This value of  $\sigma_{1D}$  is consistent with a relatively low density universe (Giovanelli et al. 1998a; Bahcall & Oh 1996; Borgani et al. 1997; Watkins 1997; Bahcall et al. 1994b; Croft & Efstathiou 1994).

#### 5. SUMMARY

We have presented T-F data and estimated the peculiar velocities of 52 rich Abell clusters spread across the sky and distributed between  $\sim 50$  and  $200 h^{-1}$  Mpc. Optical rotation curves and *I*-band photometry for 522 spiral galaxies in the fields of these systems have been obtained and presented in separate publications.

In conjunction with the robust T-F slope extracted from the relatively nearby SCI cluster sample of Giovanelli and coworkers, we find the *I*-band T-F relation to follow

$$M_I - 5 \log h = -7.68(\log W - 2.5) - 20.91 \text{ mag}.$$

The relation has an average scatter of 0.38 mag. The zero point of the T-F template has a statistical accuracy of 0.02 mag; combined with a kinematic uncertainty of 0.01 mag, which is limited by the assumption that the 52 clusters' average peculiar velocity is null, the overall uncertainty of the T-F zero point is 0.02 mag.

Peculiar velocities are obtained for each of the 52 clusters, with reference to the global template relation. The typical uncertainty on the peculiar velocity of each cluster is  $\pm 0.06cz$ , where  $cz$  is the mean cluster velocity. The rms line-of-sight component of the cluster peculiar velocity for

TABLE 4  
CLUSTER PECULIAR VELOCITIES

Cluster	$a - a_{TF}$	$cz_{helio}$	$cz_{LG}$	$cz_{CMB}$	$V_{TF,CMB}$	$V_{pec,CMB}$
A2806 .....	-0.132 (112)	8019	7918	7867	7403	464 (0382)
A114 .....	0.072 (136)	17436	17487	17144	17722	-578 (1111)
A119 .....	0.045 (160)	13470	13607	13141	13416	-275 (0988)
A2877 .....	0.032 (150)	7165	7097	6974	7078	-104 (0489)
A2877b.....	-0.075 (157)	9231	9163	9040	8733	307 (0634)
A160 .....	-0.051 (180)	12390	12577	12072	11792	280 (0977)
A168 .....	-0.116 (127)	13365	13496	13049	12370	679 (0725)
A194 .....	0.091 (125)	5343	5460	5037	5253	-216 (0302)
A260 .....	0.227 (153)	10925	11135	10664	11839	-1175 (0835)
A397 .....	-0.129 (151)	9803	9916	9594	9041	553 (0630)
A3193 .....	-0.095 (144)	10558	10381	10522	10072	450 (0668)
A3266 .....	0.307 (248)	17774	17564	17782	20482	-2700 (2345)
A496 .....	-0.129 (121)	9860	9779	9809	9243	566 (0513)
A3381 .....	-0.156 (176)	11410	11196	11510	10712	798 (0868)
A3407 .....	0.030 (205)	12714	12450	12861	13040	-179 (1235)
A569 .....	0.056 (099)	5927	5998	6011	6168	-157 (0280)
A634 .....	0.060 (125)	7822	7917	7922	8144	-222 (0469)
A671 .....	0.017 (118)	15091	15046	15307	15427	-120 (0838)
A754 .....	0.012 (426)	16282	16052	16599	16691	-92 (3294)
A779 .....	0.030 (095)	6967	6929	7211	7311	-100 (0320)
A957 .....	0.132 (144)	13464	13261	13819	14685	-866 (0974)
A1139 .....	-0.127 (119)	11851	11665	12216	11522	694 (0629)
A1177 .....	-0.011 (149)	9755	9661	10079	10028	51 (0689)
A1213 .....	-0.116 (144)	14006	13952	14304	13560	744 (0899)
A1228 .....	0.118 (099)	10517	10489	10794	11397	-603 (0517)
A1314 .....	0.029 (125)	9764	9815	9970	10104	-134 (0582)
A3528 .....	0.179 (203)	16458	16224	16770	18211	-1441 (1703)
A1736 .....	0.010 (179)	10397	10186	10690	10739	-49 (0887)
A1736b.....	-0.029 (176)	13724	13513	14017	13831	186 (1121)
A3558 .....	-0.103 (153)	14343	14122	14626	13948	678 (0981)
A3566 .....	-0.033 (118)	15370	15147	15636	15400	236 (0837)
A3581 .....	0.042 (197)	6865	6681	7122	7261	-139 (0659)
A1983b.....	-0.258 (125)	11332	11340	11524	10233	1291 (0589)
A1983 .....	-0.069 (190)	13526	13537	13715	13286	429 (1165)
A2022 .....	0.137 (125)	17262	17327	17412	18546	-1134 (1067)
A2040 .....	-0.034 (136)	13440	13429	13616	13404	212 (0839)
A2063 .....	-0.144 (087)	10444	10448	10605	9925	680 (0398)
A2147 .....	-0.063 (090)	10493	10558	10588	10285	303 (0427)
A2151 .....	-0.062 (085)	11005	11079	11093	10781	312 (0424)
A2256 .....	-0.007 (125)	17442	17673	17401	17345	56 (0998)
A2295b.....	0.047 (181)	18701	18945	18633	19041	-408 (1587)
A2295 .....	0.099 (122)	24622	24868	24554	25699	-1145 (1448)
A3656 .....	0.028 (144)	5750	5746	5586	5658	-72 (0375)
A3667 .....	0.367 (176)	16581	16491	16477	19511	-3034 (1582)
A3716 .....	-0.058 (095)	13764	13701	13618	13259	359 (0581)
A3744 .....	0.029 (111)	11386	11465	11123	11273	-150 (0578)
A2457 .....	0.018 (118)	17643	17845	17280	17424	-144 (0946)
A2572 .....	-0.084 (157)	11857	12106	11495	11059	436 (0803)
A2589 .....	0.035 (144)	12289	12531	11925	12119	-194 (0804)
A2593 .....	0.133 (102)	12415	12651	12049	12810	-761 (0605)
A2657 .....	-0.006 (157)	12028	12239	11662	11630	32 (0844)
A4038 .....	-0.017 (134)	9012	9062	8713	8645	68 (0534)

our sample, debroadened for measurement errors, is  $341 \pm 93 \text{ km s}^{-1}$ . This number agrees with that determined for the SCI sample.

The results presented here are based on observations carried out at the Palomar Observatory, at the Kitt Peak National Observatory (KPNO), the Cerro Tololo Inter-American Observatory (CTIO), and the Arecibo Observatory, which is part of the National Astronomy and Ionosphere Center (NAIC). KPNO and CTIO are operated by the Association of Universities for Research in

Astronomy, Inc., and NAIC is operated by Cornell University, all under cooperative agreements with the National Science Foundation. The Hale Telescope at the Palomar Observatory is operated by the California Institute of Technology under a cooperative agreement with Cornell University and the Jet Propulsion Laboratory. The National Radio Astronomy Observatory is a facility of the National Science Foundation operated under cooperative agreement by Associated Universities, Inc. This research was supported by NSF grants AST 94-20505 and AST 96-17069 to R. G. and AST 95-28960 to M. H.; L. E. C. was partially supported by FONDECYT grant 1970735.



## REFERENCES

- Aaronson, M., & Mould, J. 1983, *ApJ*, 265, 1
- Abell, G. O., Corwin, H. G., Jr., & Olowin, R. P. 1989, *ApJS*, 70, 1 (ACO)
- Amram, P., Sullivan, W. T., III, Balkowski, C., Marcelin, M., & Cayatte, V. 1993, *ApJ*, 403, L59
- Andreon, S. 1998, *A&A*, 336, 98
- Bahcall, N. A., Cen, R., & Gramann, M. 1994a, *ApJ*, 430, L13
- Bahcall, N. A., Gramann, M., & Cen, R. 1994b, *ApJ*, 436, 23
- Bahcall, N. A., & Oh, S. P. 1996, *ApJ*, 462, L49
- Bautz, L. P., & Morgan, W. W. 1970, *ApJ*, 162, L149
- Bernstein, G. M., Guhathakurta, P., Raychaudhury, S., Giovanelli, R., Haynes, M. P., Herter, T., & Vogt, N. P. 1994, *AJ*, 107, 1962
- Biviano, A., Giuricin, G., Mardirossian, F., & Mezzetti, M. 1990, *ApJS*, 74, 325
- Borgani, S., da Costa, L. N., Freudling, W., Giovanelli, R., Haynes, M. P., Salzer, J. J., & Wegner, G. 1997, *ApJ*, 482, L121
- Branchini, E., & Plionis, M. 1996, *ApJ*, 460, 569
- Brunozzi, P. T., Borgani, S., Plionis, M., Moscardini, L., & Coles, P. 1995, *MNRAS*, 277, 1210
- Cen, R., Bahcall, N. A., & Gramann, M. 1994, *ApJ*, 437, L51
- Courteau, S., Faber, S. M., Dressler, A., & Willick, J. A. 1993, *ApJ*, 412, L51
- Croft, R. A. C., & Efstathiou, G. 1994, *MNRAS*, 268, L23
- Dale, D. A., Giovanelli, R., Haynes, M. P., Campusano, L. E., Hardy, E., & Borgani, S. 1999a, *ApJ*, 510, L11 (Paper III)
- Dale, D. A., Giovanelli, R., Haynes, M. P., Hardy, E., & Campusano, L. E. 1999b, *AJ*, 118, 1468 (Paper IV)
- Dale, D. A., Giovanelli, R., Haynes, M. P., Scodreggio, M., Hardy, E., & Campusano, L. E. 1997, *AJ*, 114, 455 (Paper I)
- . 1998, *AJ*, 115, 418 (Paper II)
- Dressler, A., Faber, S. M., Burstein, D., Davies, R. L., Lynden-Bell, D., Terlevich, R. J., & Wegner, G. 1987, *ApJ*, 313, L37
- Eisenstein, D. J., & Loeb, A. 1996, *ApJ*, 459, 432
- Feldman, H. A., & Watkins, R. 1994, *ApJ*, 430, L17
- Giovanelli, R., & Haynes, M. P. 1985, *ApJ*, 292, 404
- Giovanelli, R., Haynes, M. P., Freudling, W., da Costa, L. N., Salzer, J. J., & Wegner, G. 1998a, *ApJ*, 505, L91
- Giovanelli, R., Haynes, M. P., Herter, T., Vogt, N. P., da Costa, L. N., Freudling, W., Salzer, J. J., & Wegner, G. 1997a, *AJ*, 113, 53 (G97a)
- Giovanelli, R., Haynes, M. P., Herter, T., Vogt, N. P., Wegner, G., Salzer, J. J., da Costa, L. N., & Freudling, W. 1997b, *AJ*, 113, 22 (G97b)
- Giovanelli, R., Haynes, M. P., Salzer, J. J., Wegner, G., da Costa, L. N., & Freudling, W. 1998b, *AJ*, 116, 2632
- Girardi, M., Escalera, E., Fadda, D., Guiricin, G., Mardirossian, F., & Mezzetti, M. 1997, *ApJ*, 482, 41
- Gramann, M., Bahcall, N. A., Cen, R., & Gott, J. R. 1995, *ApJ*, 441, 449
- Hudson, M. J. 1993, *MNRAS*, 265, 72
- Hudson, M. J., Smith, R. J., Lucey, J. R., Schlegel, D. J., & Davies, R. L. 1999, *ApJ*, 512, L79
- Iovino, A., Giovanelli, R., Haynes, M., Chincarini, G., & Guzzo, L. 1993, *MNRAS*, 265, 21
- Kogut, A., et al. 1993, *ApJ*, 419, 1
- Lahav, O., Lynden-Bell, D., & Rowan-Robinson, M. 1988, *MNRAS*, 234, 677
- Lauer, T. R., & Postman, M. 1994, *ApJ*, 425, 418 (LP)
- Lynden-Bell, D., Faber, S. M., Burstein, D., Davies, R. L., Dressler, A., Terlevich, R. J., & Wegner, G. 1988, *ApJ*, 326, 19
- Lynden-Bell, D., Lahav, O., & Burstein, D. 1989, *MNRAS*, 241, 325
- Marinoni, C., Monaco, P., Giuricin, G., & Costantini, B. 1998, *ApJ*, 505, 484
- Mathewson, D. S., Ford, V. L., & Buchhorn, M. 1992, *ApJS*, 81, 413
- Peebles, P. J. E. 1993, *Principles of Physical Cosmology* (Princeton: Princeton Univ. Press)
- Plionis, M., & Kolokotronis, V. 1998, *ApJ*, 500, 1
- Riess, A. G., Press, W. H., & Kirshner, R. P. 1995, *ApJ*, 445, L91
- Roberts, M. S. 1978, *AJ*, 83, 1026
- Roberts, M. S., & Haynes, M. P. 1994, *ARA&A*, 32, 115
- Rowan-Robinson, M., et al. 1990, *MNRAS*, 247, 1
- Rubin, V. C., Ford, W. K., Jr., & Whitmore, B. C. 1988, *ApJ*, 333, 522
- Rubin, V. C., Roberts, M. S., Thonnard, N., & Ford, W. K., Jr. 1976, *AJ*, 81, 719
- Sandage, A. 1994a, *ApJ*, 430, 1
- . 1994b, *ApJ*, 430, 13
- Sandage, A., Tammann, G. M., & Federspiel, M. 1995, *ApJ*, 452, 1
- Sarazin, C. L. 1986, *Rev. Mod. Phys.*, 58, 1
- Scaramella, R., Vettolani, G., & Zamorani, G. 1994, *ApJ*, 422, 1
- Schechter, P. L. 1980, *AJ*, 85, 801
- Strauss, M. A., Cen, R., Ostriker, J. P., Lauer, T. R., & Postman, M. 1995, *ApJ*, 444, 507
- Strauss, M. A., Yahil, A., Davis, M., Huchra, J. P., & Fisher, K. 1992, *ApJ*, 397, 395
- Tammann, G. A. 1999, in *The Eighth Marcel Grossman Meeting*, ed. T. Piran (Singapore: World Sci.), in press
- Tammann, G. A., & Sandage, A. 1985, *ApJ*, 294, 81
- Teerikorpi, P. 1997, *ARA&A*, 35, 101
- Vogt, N. P. 1995, Ph.D. thesis, Cornell Univ.
- Watkins, R. 1997, *MNRAS*, 292, L59
- Watkins, R., & Feldman, H. A. 1995, *ApJ*, 453, L73
- Whitmore, B. C., Forbes, D. A., & Rubin, V. C. 1988, *ApJ*, 333, 542
- Willick, J. A. 1990, *ApJ*, 351, L5
- . 1994, *ApJS*, 92, 1
- . 1999, *ApJ*, 516, 47
- Willick, J. A., Courteau, S., Faber, S. M., Burstein, D., & Dekel, A. 1995, *ApJ*, 446, 12
- Willick, J. A., Courteau, S., Faber, S. M., Burstein, D., Dekel, A., & Strauss, M. A. 1997, *ApJS*, 109, 333
- Zehavi, I., Riess, A. G., Kirshner, R. P., & Dekel, A. 1998, *ApJ*, 503, 483